

Journal of Materials Chemistry A

Accepted Manuscript



This is an *Accepted Manuscript*, which has been through the Royal Society of Chemistry peer review process and has been accepted for publication.

Accepted Manuscripts are published online shortly after acceptance, before technical editing, formatting and proof reading. Using this free service, authors can make their results available to the community, in citable form, before we publish the edited article. We will replace this *Accepted Manuscript* with the edited and formatted *Advance Article* as soon as it is available.

You can find more information about *Accepted Manuscripts* in the [Information for Authors](#).

Please note that technical editing may introduce minor changes to the text and/or graphics, which may alter content. The journal's standard [Terms & Conditions](#) and the [Ethical guidelines](#) still apply. In no event shall the Royal Society of Chemistry be held responsible for any errors or omissions in this *Accepted Manuscript* or any consequences arising from the use of any information it contains.



Journal Name

ARTICLE

Scaffolding an Ultrathin CdS Layer on ZnO Nanorods Array using Pulsed Electrodeposition for Improved Photocharge Transport under Visible Light Illumination

Received 00th January 20xx,
Accepted 00th January 20xx

DOI: 10.1039/x0xx00000x

Yiming Tang, Patrapark Traveerungroj, Hui Ling Tan, Peng Wang, Rose Amal[†] and Yun Hau Ng[†]

www.rsc.org/

An ultrathin layer of CdS (~8 nm) was successfully coated on an array of vertically aligned ZnO nanorods using pulsed electrodeposition. The pulse was essential during the deposition of CdS to ensure equilibrium between diffusion and nucleation of CdS precursors. These ZnO nanorods functioned as a large contact base for the deposition of CdS. This enlarged interface between CdS and ZnO together with its close intimacy facilitated efficient charge transfer from the excited CdS to ZnO upon visible illumination. Owing to the high electron mobility of ZnO, it shuttled the electrons efficiently for enhanced photocurrent generation. Compared to bare CdS film, the CdS-ZnO photoelectrode yielded a doubled anodic visible photocurrent density of 6 mA/cm² at 0 V vs. Ag/AgCl. Photoluminescence spectroscopy and photoelectrochemical characterizations showed that the charge recombination within CdS was suppressed and the proper band alignment favored the electron transfers.

Introduction

Metal chalcogenides represent an attractive class of photoactive semiconductors as they generally exhibit narrow optical band gap which is responsive to visible light of the solar spectrum.¹⁻³ Cadmium sulfide (CdS) is one of the most investigated metal chalcogenides that has a direct band gap of ~ 2.4 eV. Together with its highly energetic conduction band (ca -1.0 V vs NHE) and reasonably high electrons density at room temperature, CdS has demonstrated its potential in photocatalytic and photoelectrochemical applications.⁴ Typically, CdS has found uses in photocatalysis, photovoltaic, photodetector, sensors etc.⁵⁻⁸ In photocatalysis, nanoparticles of CdS are generally used in the form of suspension in aqueous solution. CdS nanoparticles with various sizes, morphological structures, and surface chemical properties have been designed to achieve larger surface area, better charge transport, and higher photostability.⁹⁻¹⁰ Other than photocatalysis, most of the above mentioned applications involve the use of CdS thin film rather than nanoparticles/powder. Coating CdS powder onto a suitable flat substrate with the aide of chemical binder or heat treatment appears to be a convenient way to construct CdS thin film

although it often encounters film stability (adhesion) issue.¹¹ Other options to fabricate CdS thin film without pre-synthesizing the nanoparticles include chemical vapor deposition, vacuum evaporation, sputtering, spray pyrolysis, successive ionic layer adsorption and reaction, chemical bath deposition and electrodeposition.¹²⁻¹⁶ Because electrodeposition is a low cost method, scalable for large thin film synthesis and involves only simple setup of instrumentation, it has been widely used to prepare metal-based thin films including CdS.¹⁷ A high quality thin film of CdS with good homogeneity can be conveniently electrodeposited using an aqueous solution containing Cd salt and thiosulfate as the source of sulfur.¹⁸ The photoresponse of CdS thin films is depending on the photocharge transportation from CdS to the charge collecting substrate upon photoexcitation. In most cases, the transparent indium-doped tin oxide (ITO) and fluorine-doped tin oxide (FTO) are used as the charge collecting substrates. Although stable visible photoresponse from CdS thin film has been achieved,⁹ the photocharge transportation is regulated by the film thickness (i.e. film thickness should be shorter than the charge diffusion length of CdS) and the efficiency of the charge collection at the substrate.

In order to improve the charge collection at the substrate, maximizing the charge collection site is favorable and it can be achieved by transforming the flat substrate into porous or anisotropic nanostructure such as one-dimensional (1D) nanotubes, nanorods, nanoneedles etc.¹⁹⁻²² These non-flat substrates serve as large contact base for the deposition of CdS which facilitate more interfaces for charge transfer.

Particles and Catalysis Research Group, School of Chemical Engineering
The University of New South Wales
Sydney NSW 2052, Australia

[†]E-mail: r.amal@unsw.edu.au; yh.ng@unsw.edu.au

Electronic Supplementary Information (ESI) available: [XRD patterns of FTO substrate, CdS film and CdS-ZnO film from pulsed electrodeposition, SEM images, PEC of CdS-ZnO from non-pulsed electrodeposition, absorption spectra of pristine ZnO, pure CdS and CdS-ZnO and onset potential of CdS and CdS-ZnO are available]. See DOI: 10.1039/x0xx00000x

Vertically aligned ZnO nanorods array grown on FTO is a good candidate for this purpose as ZnO possesses greater electron mobility than many other oxide nanostructures.²³⁻²⁴ This 1D ZnO nanorods array can be prepared by a number of methods enabled by the advancement in the chemical synthesis today. However, the challenge lies in the high quality deposition of CdS onto them. The conventional electrodeposition method offers good versatility in preparing an even deposit film on flat substrate but it has limitation to coat the vertically aligned 1D nanostructured substrates. The presence of concentration gradient of the precursor, i.e. higher precursor concentration at the upper layer of the 1D nanostructure compared with the bottom region, always result in dominant deposit at the top layer of the 1D nanostructured substrate and considerably uncoated bottom part. The situation can be even more challenging when each single nanorod/nanotube is too close to each other to impose capillary resistance for the diffusion of precursors. In this work we develop a square-wave pulsed electrodeposition method to overcome the above difficulties in depositing an even layer of CdS over the wall of the vertically aligned ZnO nanorods substrate.

Nonetheless, CdS nanoparticles have been previously decorated onto 1D TiO₂ nanotubes and 1D ZnO nanorods thin film with different level of coating quality using single-step electrodeposition, sequential chemical bath deposition and ion-exchange approach.²⁵⁻²⁷ The purpose of composing CdS-ZnO and CdS-TiO₂ in those earlier studies was to facilitate extension of light absorption into visible light region. The visible light photocurrent generation of CdS-ZnO (or CdS-TiO₂) was found greatly enhanced compared with the bare ZnO (or TiO₂). While ZnO and TiO₂ have band gap > 3.0 eV which corresponding to UV-excitation, the sensitization with narrow band gap CdS component was therefore expected to generate visible light response. However, it remains unclear that if CdS-ZnO will be more superior to the bare CdS thin film under visible illumination because the geometry of CdS-ZnO and the interfaces between them may affect the excitation and charge transport of the excited CdS. In this work, we aim to improve the performance of visible light response CdS by evenly anchoring them onto the anisotropic ZnO nanorods array which is vertically aligned on FTO glass substrates. ZnO nanorods provide larger charge collecting area for the deposited CdS. The thin CdS layer has thickness less than its charge diffusion length; therefore the excited charges from CdS are extracted more efficiently into ZnO. Together with the close intimacy with ZnO and the large contact interface provided by the anisotropic 1D structure, CdS-ZnO thin film has photoelectrochemical performance 100% higher than the pulsed electrodeposited bare CdS thin film under visible light. The photocurrent density obtained in this work is in general higher than the reported values under the similar measurement conditions.^{10, 28} Notably, ZnO in this work was not involved actively in generating electron (as it is not photoexcited) but served as the electron mediator and effective scaffold for CdS deposition. The importance of providing large collecting site for charges further equipped

with high quality deposition to ensure efficient electron flow is demonstrated.

Experimental Section

Preparation of a ZnO nanorod film on a FTO substrate

ZnO nanorod films were prepared by a chemical bath deposition (CBD) method on FTO substrates. All FTO substrates were pre-cleaned with Milli-Q water, ethanol (99.5%, Sigma-Aldrich) and acetone (99.8%, Chem-Supply) under mild sonication followed by drying in air. ZnO seeding layers on the cleaned FTO substrates were formed by thermal decomposition of zinc acetate before CBD process. Several drops of a solution containing 0.005 M of zinc acetate (Ajax Finechem) dissolved in ethanol were applied on the transparent FTO substrates. After 10 seconds, the substrates were rinsed with ethanol and dried with nitrogen gas. The wetting process with zinc acetate was repeated for five times before calcined for 20 min at 350 °C to form ZnO seeds from thermal decomposition of zinc acetate. The whole seeding procedure was repeated for two times to obtain evenly distributed ZnO seed layers on the FTO substrates.

The seeded substrates were then sealed in a Schott bottle with 100 mL aqueous solution consisted of 0.025 M of zinc nitrate (98%, Sigma-Aldrich) and 0.025 M of hexamethylenetetramine (99%, Sigma-Aldrich) used as a structure-directing agent. Each solution was preheated to 90°C for 5 min before mixing. The bottle was then kept in the oven at 90°C for 3 h. This growth cycle was repeated twice. The obtained ZnO nanorod thin films were rinsed thoroughly in Milli-Q water and dried in air. Subsequently, the transparent ZnO nanorod films were calcined for 30 min at 450 °C to completely remove the remaining organic components.

Preparation of CdS nanoparticles on the ZnO nanorod film

CdS nanoparticles on a FTO substrate and the ZnO nanorod film were deposited by a pulsed electrodeposition method in a three-electrode cell, with a FTO substrate and the resultant ZnO nanorod film as the working electrodes, Ag/AgCl as a reference electrode and a Pt foil as the counter electrode. A mixture of 10 mM CdCl₂ and 100 mM Na₂S₂O₃ was chosen as the electrolyte. The excess sulphur source was to secure the stoichiometric ratio of Cd and S considering the sulphur loss in the following calcination process. The CdS nanoparticles was deposited electrochemically at ambient temperature by applying a rectangular current waveform imposing in a periodic manner generated by a Potentiostat (Metrohm Autolab PGSTAT M101, MEP instruments) combined with Nova software, applying a cathodic pulse (-1.25 V, 5 ms – 0.5 s) and short-circuit pulse (0 V, 5 ms – 0.5 s) alternatively for 30 min. The voltage, frequency and duration values are carefully chosen based on the optimized conditions. The-obtained CdS-ZnO film was dried and calcined at 400 °C for 30 min in N₂ in a horizontal quartz tube furnace (HTFS80-450/1, Labec) to facilitate crystallisation. Before the heating, N₂ was purged

through the tube furnace for 2 h to completely remove the air. Subsequently, the heating was performed with the ramping rate of 5 °C/min from room temperature to 400°C. The gas flow rate was maintained at 50 mL/min throughout the process.

Characterization of the obtained CdS-ZnO composites

The crystallographic phase structures of the deposited films were characterized using an X-ray diffractometer (X'pert Pro MRD, Philips) with Cu K α radiation at 45 kV and 40 mA, a step size of 0.013° and a scan step time at 97.92 s in the 2 θ range of 20° to 60°. The morphological features and the film thickness were determined using a scanning electron microscope (Nova NanoSEM 230, FEI). The UV-Vis diffuse reflectance spectra were obtained using a UV/Vis/NIR spectrophotometer (UV-3600 Plus, Shimadzu). A high-resolution transmission electron microscopy (HRTEM, CM200 Philips) was employed to examine the lattice fringes of electrodeposited CdS and ZnO crystals, as well as the interface between the CdS nanoparticles and the ZnO nanorod film. The Mott–Schottky plots of the ZnO, CdS and CdS-ZnO film were measured using a potentiostat (Metrohm Autolab PGSTAT 302N, MEP instruments) combined with a frequency response analyzer (Autolab FRA2 modules) with a frequency of 700 Hz scanning from -1.5 V to 0 V (vs. Ag/AgCl) at a scan rate 50 mV/s. The photoluminescence emission spectra were obtained using a spectrometer (FluoroMax-4, Horiba) to study the recombination rate of electrons and holes within the film.

The photoelectrochemical properties of the ZnO, CdS and CdS-ZnO films were examined under potentiostatic conditions in a three-electrode system using CdS-ZnO films as the working electrode, Ag/AgCl as the reference electrode and a platinum wire as the counter electrode in an aqueous solution containing 0.25 M of Na₂S and 0.35 M of Na₂SO₃ at pH 12. An electrolytic cell made out of Teflon with a flat quartz window was used. The photocurrent responses were measured under visible light illumination using a 300 W Xenon lamp with a cut off filter ($\lambda \geq 435$ nm). The illuminated area of the working electrode was fixed at 0.196 cm².

Results and discussion

Upon pulsed-electrodeposition at -1.25 V with frequency of 100 Hz, a homogeneous yellow layer was found evenly coated on FTO substrate (Figure 1a). Examination under a scanning electron microscope (SEM, Figure 1b) reveals the morphology of this evenly coated layer consists of fused nanoparticles with comparable primary particle size of ca 20 – 30 nm. Voids or pores are present within the spaces among each cluster of fused nanoparticles. This morphological feature of pulsed-electrodeposited CdS film is different from the reported electrodeposited CdS film in which a compact film with undeveloped porosity was a common observation.^{29,30} It is believed that porous CdS film may have enhanced electron conduction because more CdS-electrolyte interfaces are

created. Figure 1c and d show that these irregularly-shaped nanoparticles have visible light response with the onset light absorption wavelength at 520 nm which is corresponding to the band gap of CdS (ca. 2.4 eV). The absorbance of CdS film has extended to visible light range compared to that of ZnO nanoarrays. High resolution transmission electron microscopy (HRTEM) image in Figure 1e confirms that the nanoparticles are the crystalline CdS exhibiting (001) facet with lattice fringe of 0.34 nm. The pulsed-electrodeposited film was also verified by x-ray diffraction (XRD) to consist of crystalline CdS with the diffraction peaks at 24.8° and 28.2° to represent (100) and (101) planes of the hexagonal CdS, respectively (see Figure S1 in Supporting Information).

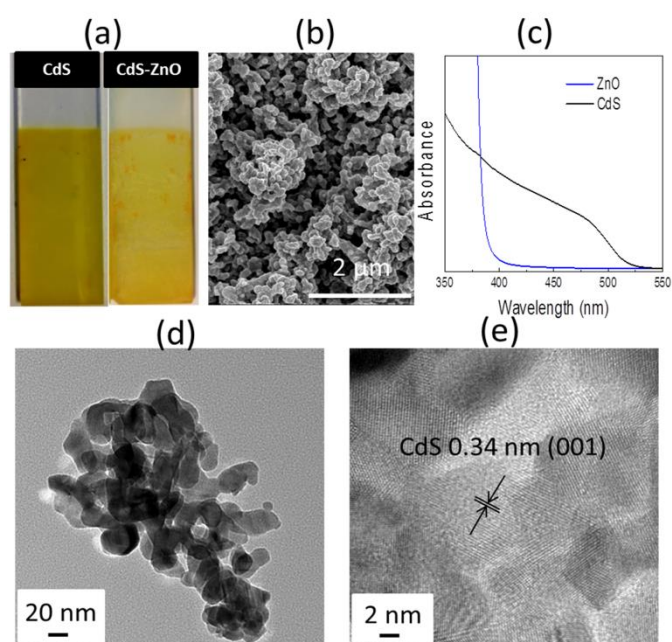


Figure 1. (a) CdS film on a FTO substrate and a ZnO substrate from pulsed electrodeposition; (b) SEM image of CdS thin film on the FTO substrate using pulsed electrodeposition; (c) Absorption spectra of CdS thin film on the FTO substrate from pulsed electrodeposition and ZnO nanoarrays from chemical bath deposition; (d) TEM image of CdS nanoparticles on the FTO substrate from pulsed electrodeposition; (e) HRTEM of CdS film on the FTO substrate from pulsed electrodeposition.

Vertically aligned ZnO nanorods array on FTO is an ideal scaffold to support CdS when compare to the flat FTO substrate as it provides larger anchoring sites for CdS. Figure 2a shows the typical morphology of ZnO nanorods prepared using chemical bath deposition (CBD) method. The hexagonal nanoarrays with smooth surface are observed with consistent diameter of ca. 80 nm. Employing the identical pulsed-electrodeposition condition used for the bare CdS thin film, it is clearly seen that the surface of ZnO nanorods is completely covered by a thin but rough layer of nanoparticles (Figure 2b). Photograph of this CdS-ZnO thin film (Figure 1a) also suggests the uniform deposition of CdS across the thin film. Microscopically, overall diameter of the nanorods is not noticeably changed because of the ultra-thin coating. It is worth to note that conventional electrodeposition (i.e. non-

pulsed electrodeposition) has not been reported to successfully wrap 1D-nanoarray substrate. As shown in Figure S2a (Supporting Information), non-pulsed electrodeposition led to the formation of relatively thick CdS layer on top of the ZnO nanoarrays without penetrating into the bottom region of the film. This over-layer of deposited component on the 1D-nanoarrays was typically observed in previous studies (e.g. CuInS₂ nanoparticles on TiO₂ nanotubes array).^{31,32}

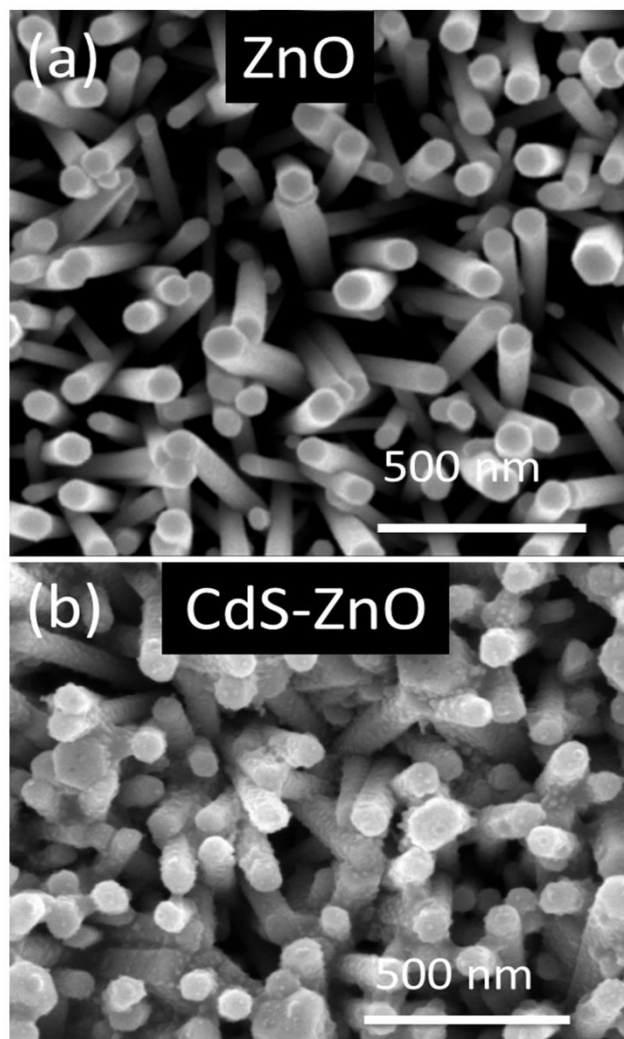


Figure 2. (a) SEM image of ZnO nanorod film from 6 h of chemical bath deposition; (b) SEM image of CdS-ZnO composite from pulsed electrodeposition.

Figure 3 shows the images of transmission electron microscope (TEM) and high resolution TEM (HRTEM) obtained on the ZnO and CdS-ZnO powder scratched off from the FTO substrate. In consistent with the SEM analysis, clean surface of bare ZnO with well-defined lattice fringe (0.26 nm, corresponding to (001) facet) was observed. In contrast, a homogeneous coating layer on ZnO with an even thickness of ca. 8 nm is found on CdS-ZnO nanorods sample. The magnified area of the typical interface between ZnO and CdS exhibits the presence of crystalline ZnO and CdS. It is also noted that the size of CdS nanoparticles is smaller in CdS-ZnO (8-10 nm) than in the bare CdS (20-30 nm) film. This is an expected difference

between the two films because ZnO nanorods provide larger nucleation site for electrodeposition of fresh CdS. However, in bare CdS film, the CdS precursors were electrodeposited and grown on the existing CdS crystal to yield larger particles. UV-visible absorption spectra of CdS-ZnO (Figure S3 in Supporting Information) and bare CdS films show identical onset wavelength at 520 nm, indicating the similar optical band gap possessed by both samples. Thus, quantum size effect induced by small sized-CdS is not observed in the studied particle size range.

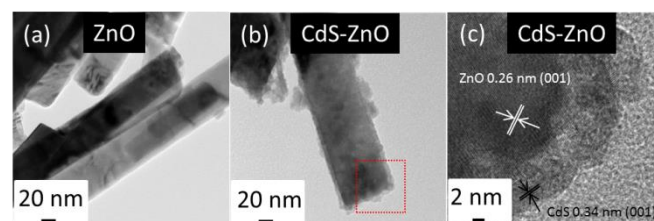


Figure 3. (a) TEM image of ZnO nanorod film from chemical bath deposition; (b) TEM image of CdS-ZnO composite from pulsed electrodeposition; (c) HRTEM image of CdS-ZnO composites from pulsed electrodeposition.

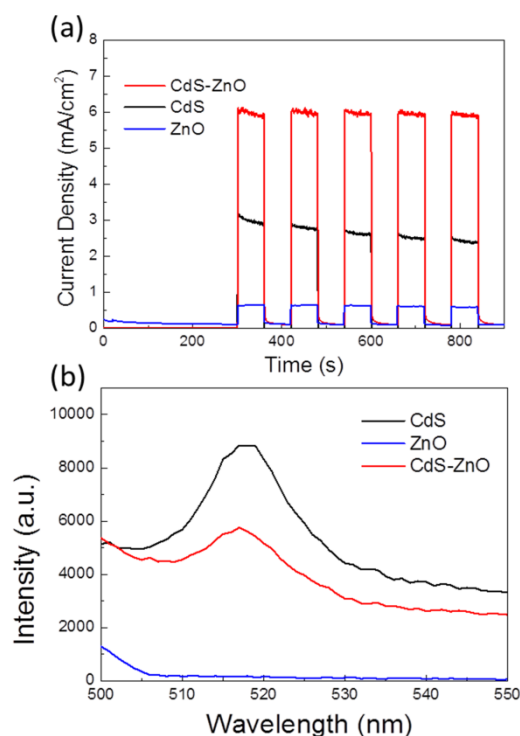


Figure 4. (a) PEC measurements of ZnO, CdS and CdS-ZnO composite from pulsed electrodeposition at 0 V vs. Ag/AgCl in an electrolyte containing 0.25 M Na₂S and 0.35 M Na₂SO₃ (pH = 12) under chopped visible light irradiation ($\lambda \geq 435$ nm); (b) Emission photoluminescence (PL) spectra (excitation wavelength 425 nm) of pristine ZnO, pure CdS and CdS-ZnO composites films from pulsed electrodeposition.

Photoelectrochemical (PEC) performances of the pulsed-electrodeposited bare CdS and CdS-ZnO films were evaluated under visible light (>420 nm) at a constant bias of 0 V vs Ag/AgCl (Figure 4a). At 0 V where the photocurrent is mainly driven by the intrinsic electron transport properties of the CdS, it is shown that CdS pulsed-deposited on ZnO has a higher

anodic photocurrent density of 6 mA/cm^2 compared with the bare CdS pulsed-electrodeposited on FTO (2.8 mA/cm^2). Note that the value of photocurrent density for CdS-ZnO is higher than the reported value yielded by conventional non-pulsed electrodeposition. For example, CdS-ZnO film obtained from non-pulse system in this work generated photocurrent density of 3.5 mA/cm^2 (Figure S2b in Supporting Information). Although photocurrent increment over the bare CdS counterpart is still observed and attributed to the improved charge transfer to the substrate (ZnO), its absolute activity is inferior to the pulsed electrodeposited CdS-ZnO. Photocurrents of CdS-ZnO obtained from pulsed-electrodeposition with different durations are also shown in Figure S4 as reference. While UV-Vis spectra indicated comparable absorbance under visible illumination, the high photocurrent density of CdS-ZnO is promoted by the larger charge collection sites facilitated by the ZnO nanorods arrays. A more efficient mechanism in transferring the electrons from the excited CdS results in less charge recombination in the film. Figure 4b shows the photoluminescence (PL) spectra of CdS and CdS-ZnO films. Photoluminescence is emitted when the excited electrons return to their ground state (recombination phenomenon). Therefore the intensity of the PL emission peak reflects the significance of charge recombination. The emission peak at 518 nm is also indicative of the optical band gap of CdS component in the composite film. The obvious quenching of PL emission band of CdS-ZnO verifies the reduced charge recombination which contributed to the enhanced PEC performances. Bare ZnO film did not generate PL emission peak under the excitation source of 425 nm.

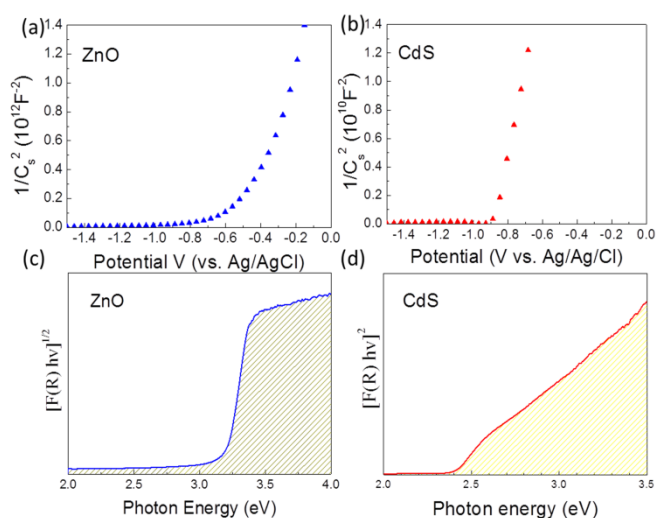


Figure 5. (a) Mott-Schottky plots of ZnO film from chemical bath deposition; (b) CdS film from pulsed electrodeposition, the capacity measurements of (a) and (b) were carried out at 700 Hz within the potential range of -1.5 V to 0 V vs. Ag/AgCl; (c) Tauc plot of ZnO film from chemical bath deposition; (d) Tauc plot of CdS film from pulsed electrodeposition.

The presence of smaller CdS nanoparticles and its thin coating over ZnO nanorods facilitated a more favorable charge migration pathway where the thickness of CdS ($\sim 8 \text{ nm}$) is shorter than its electron diffusion length.³³ The intimacy of CdS

and ZnO also enabled the electron transfer and more importantly, this charge transfer is powered by the suitable band energy alignment present at the interface. Figure 5 shows the Mott-Schottky (top panel) and Tauc plots (bottom panel) of ZnO and CdS. Tauc plot of the CdS-ZnO is included in Figure S5 for reference. Mott-Schottky analyses measured the flat band potentials of the semiconductors while valence band potentials could be derived after the optical band gaps measured in Tauc plot are taken into consideration.³⁴ Based on the Mott-Schottky plots, the observed positive slopes of the capacitance against voltage verify that both ZnO and CdS as n-type semiconductors. The extrapolation of the linear region of the slope evaluates the flat band potentials of both materials. As flat band potentials for n-type semiconductors are generally located slightly below the conduction bands, the intercept value at x-axis can be used to estimate the conduction band potentials. Derived from Nernst equation,³⁵ the flat band potentials of ZnO and CdS are calculated to be -0.25 and -0.34 V vs RHE, respectively. These values are in good agreement with the literature reports.³⁶ Because both CdS and ZnO have n-type conductivity, the higher level of conduction band of CdS (more negative) forms a proper energy alignment with ZnO in which the photoexcited electron in CdS can be favorably transferred to ZnO to achieve higher efficiency of electrons transportation.

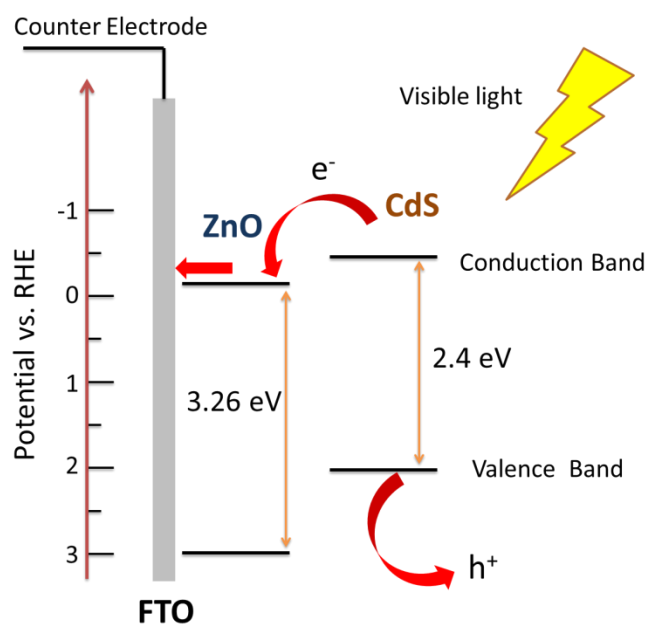


Figure 6. Schematic of band structures of CdS-ZnO composites³⁷

As ZnO and CdS possess optical band gap of 3.2 and 2.4 eV, respectively, as measured in Tauc analyses, an energy diagram of the CdS-ZnO composite is constructed accordingly in Figure 6. Visible light-excited CdS has a pool of electrons that thermodynamically tend to be transferred to ZnO thus minimizing charge recombination within CdS. The transfer of electrons from CdS to ZnO is also supported by the observation of the slight positive shift in the onset potential

for photocurrent generation (Figure S6 in Supporting Information).³⁸ With the high electron mobility characteristic of ZnO, these electrons are further shuttled to FTO and extracted away to generate photocurrent. Although the principle is similar with the sensitization of ZnO, this study proves that the photoactivities of non-supported CdS were doubled because of the introduction of 1D-nanostructured scaffold. Larger CdS-ZnO interface area facilitated by 1D ZnO nanorods together with the finely dispersed thin layer of CdS contributed to the enhancement observed in CdS-ZnO against bare CdS thin film.

Conclusions

In conclusion, ZnO nanorods arrays vertically aligned on conducting substrate can be used as a suitable large area scaffold to support CdS for improved visible light photoelectrochemical performances. The high quality thin layer coating of CdS is effectively achieved by introducing an optimized pulse frequency during the electrodeposition. The enlarged interface area between CdS and ZnO, the thin layer of CdS which consists of fine nanoparticles and the perfect wrapping of ZnO by CdS are responsible for the 100% enhancement in the photoelectrochemical performances of the pulsed-electrodeposited CdS-ZnO. This work is therefore providing alternative strategy to improve photoelectrode performance through interface engineering.

Acknowledgements

This work has been supported by the Australian Research Council Discovery Project (DP110101638). Yiming Tang acknowledges the China Scholarship Council scholarship. The authors also would like to acknowledge the UNSW Mark Wainwright Analytical Centre for the SEM and TEM equipment, especially Mrs Sigrid Fraser and Dr. Rhiannon Kuchel for their generous help.

Notes and references

- C. H. Lai, M. Y. Lu, L. J. Chen, *J. Mater. Chem.*, 2012, **22**, 19;
- K.-W. Cheng, Y.-C. Wu, Y.-T. Hu, *Mater. Res. Bull.*, 2013, **48**, 2457;
- K. Iwashina, A. Iwase, Y. H. Ng, R. Amal, A. Kudo, *J. Am. Chem. Soc.*, 2015, **137**, 604.
- B. Pödör, J. Balázs, M. Hársy, *Phys. Stat. Sol. (a)*, 1971, **8**, 613.
- X. Wang, G. Liu, G. Q. Lu, H.-M. Cheng, *Int. J. Hydrogen Energy*, 2010, **35**, 8199.
- T. L. Chu, S. S. Chu, N. Schultz, C. Wang, C. Q. Wu, *J. Electrochem. Soc.*, 1992, **139**, 2443.
- K. Deng, L. Li, *Adv. Mater.*, 2014, **26**, 2619;
- E. D. Spörke, M. T. Lloyd, Y. J. Lee, T. N. Lambert, B. B. McKenzie, Y. B. Jiang, D. C. Olson, T. L. Sounart, J. W. P. Hsu, J. A. Voigt, *J. Phys. Chem. C*, 2009, **113**, 16329.
- W. Kim, M. Seol, H. Kim, J. B. Miller, A. J. Gellman, K. Yong, *J. Mater. Chem. A*, 2013, **1**, 9587.
- Y. Xu, W. Zhao, R. Xu, Y. Shi, B. Zhang, *Chem. Commun.*, 2013, **49**, 9803.
- Pareek, P. Paik, P. H. Borse, *Langmuir*, 2014, **30**, 15540.
- J. P. Ge, Y. D. Li, *Adv. Funct. Mater.*, 2004, **14**, 157.
- M. Tomakin, M. Altunbas, E. Bacaksiz, S. Celik, *Thin Solid Films*, 2012, **520**, 2532.
- N. Romeo, A. Bosio, V. Canevari, D. Seuret, *Solar Cells*, 1987, **22**, 23.
- Y. Y. Ma, R. H. Bube, *J. Electrochem. Soc.*, 1977, **124**, 1430.
- P. K. Nair, M. T. S. Nair, V. M. Garcia, O. L. Arenas, Y. Pena, A. Castillo, I. T. Ayala, O. Gomezdaza, A. Sanchez, J. Campos, H. Hu, R. Suarez, M. E. Rincon, *Sol. Energ. Mater. Sol. Cells*, 1998, **52**, 313.
- D. G. Diso, G. E. A. Muftah, V. Patel, I. M. Dharmadasa, *J. Electrochem. Soc.*, 2010, **157**, H647.
- S. J. Lade, M. D. Uplane, C. D. Lokhande, *Mater. Chem. Phys.*, 1998, **53**, 239.
- Y. Q. Qu, X. F. Duan, *J. Mater. Chem*, 2012, **22**, 16171.
- S. Emin, M. Fanetti, F. F. Abdi, D. Lisjak, M. Valant, R. van de Krol, B. Dam, *ACS Appl. Mater. Interfaces.*, 2013, **5**, 1113.
- D. R. Baker, P. V. Kamat, *Adv. Funct. Mater.*, 2009, **19**, 805.
- Z. Zheng, W. Xie, Z. S. Lim, L. You, J. Wang, *Sci. Rep.*, 2014, **4**, 5721.
- K. Keis, L. Vayssieres, H. Rensmo, S. E. Lindquist, A. Hagfeldt, *J. Electrochem. Soc.*, 2001, **148**, A149.
- G. Yang, W. Yan, Q. Zhang, S. Shen, S. Ding, *Nanoscale*, 2013, **5**, 12432.
- S. Banerjee, S. K. Mohapatra, P. P. Das, M. Misra, *Chem Mater Chem. Mater.*, 2008, **20**, 6784.
- W. T. Sun, Y. Yu, H. Y. Pan, X. F. Gao, Q. Chen, L. M. Peng, *J. Am. Chem. Soc.*, 2008, **130**, 1124.
- J. G. Jiang, M. Wang, L. J. Ma, Q. Y. Chen, L. J. Guo, *Int. J. Hydrogen. Energy*, 2013, **38**, 13077.
- L. H. Zhu, C. Li, Y. J. Li, C. H. Feng, F. Li, D. Z. Zhang, Z. G. Chen, S. P. Wen, S. P. Ruan, *J. Mater. Chem. C* 2015, **3**, 2231.
- S. Dennison, *Electrochim. Acta.*, 1993, **38**, 2395.
- J. Azevedo, C. T. Sousa, A. Mendes, J. P. Araujo, *J. Nanosci. Nanotechnol.*, 2012, **12**, 9112.
- J. H. Yun, Y. H. Ng, S. Huang, G. Conibeer, R. Amal, *Chem. Commun.*, 2011, **47**, 11288.
- Y. Tang, J. H. Yun, L. Wang, R. Amal, Y. H. Ng, *Dalton Trans.*, 2015, **44**, 7127.
- X. Qi, G. She, Y. Liu, L. Mu, W. Shi, *Chem. Commun.*, 2012, **48**, 242.
- Y. Tang, Y. H. Ng, J. H. Yun, R. Amal, *RSC Adv.*, 2014, **4**, 3278.
- S. J. Hong, S. Lee, J. S. Jang, J. S. Lee, *Energ. Environ. Sci.*, 2011, **4**, 1781.
- M. Gratzel, *Nature*, 2001, **414**, 338.
- S. Hotchandani, P. V. Kamat, *J. Phys. Chem.*, 1992, **96**, 6834.
- C. Ng, A. Iwase, Y. H. Ng, R. Amal, *J. Phys. Chem. Lett.*, 2012, **3**, 913.